

SCIENTIFIC REPORTS

OPEN

Effect of Low-Temperature Al₂O₃ ALD Coating on Ni-Rich Layered Oxide Composite Cathode on the Long-Term Cycling Performance of Lithium-Ion Batteries

Sven Neudeck¹, Andrey Mazilkin^{1,2,3,4}, Christian Reitz^{2,3}, Pascal Hartmann^{1,5}, Jürgen Janek^{1,6} & Torsten Brezesinski¹

Conformal coating of nm-thick Al₂O₃ layers on electrode material is an effective strategy for improving the longevity of rechargeable batteries. However, solid understanding of how and why surface coatings work the way they do has yet to be established. In this article, we report on low-temperature atomic layer deposition (ALD) of Al₂O₃ on practical, ready-to-use composite cathodes of NCM622 (60% Ni), a technologically important material for lithium-ion battery applications. Capacity retention and performance of Al₂O₃-coated cathodes (≤ 10 ALD growth cycles) are significantly improved over uncoated NCM622 reference cathodes, even under moderate cycling conditions. Notably, the Al₂O₃ surface shell is preserved after cycling in full-cell configuration for 1400 cycles as revealed by advanced electron microscopy and elemental mapping. While there are no significant differences in terms of bulk lattice structure and transition-metal leaching among the coated and uncoated NCM622 materials, the surface of the latter is found to be corroded to a much greater extent. In particular, detachment of active material from the secondary particles and side reactions with the electrolyte appear to lower the electrochemical activity, thereby leading to accelerated capacity degradation.

Ni-rich layered lithium transition-metal oxides, in particular LiNi_{0.80}Co_{0.15}Al_{0.05}O₂ (NCA) and Li_{1+x}(Ni_{1-y-z}Co_yMn_z)_{1-x}O₂ (NCM, $\geq 60\%$ Ni), are emerging as cathode active materials (CAMs) of choice for application in rechargeable lithium-ion batteries (LIBs) for electric vehicles^{1,2}. Further optimization of these materials involves improving their mechanical and structural stability and suppressing side reactions such as corrosion. To this end, both bulk doping and coating the surface of secondary particles by a thin shell have been shown to be effective strategies³⁻⁵. Among the various types of coating materials that have been applied to CAMs, aluminum oxide (Al₂O₃) is by far the most prominent and widely used, not only in academia but also industry.

In general, Al₂O₃ can be prepared by solution (wet) chemistry⁶⁻¹⁰ or, as shown in recent years, via atomic layer deposition (ALD)¹¹⁻¹⁴. Al₂O₃ ALD is a well-established process, usually consisting of two half-reaction steps using trimethylaluminum (TMA) and H₂O, respectively, as the reactants. Major advantages of ALD over other techniques are the ability to produce conformal coating layers and the high degree of control over their thickness¹⁵⁻¹⁷. In most cases, ALD is applied to CAM powder as shown, for example, for LiCoO₂ (LCO)¹⁸⁻²² and NCM²³⁻²⁷. However, ALD also offers the possibility to perform the coating directly on ready-to-use electrodes as reported for

¹Battery and Electrochemistry Laboratory, Institute of Nanotechnology, Karlsruhe Institute of Technology (KIT), Hermann-von-Helmholtz-Platz 1, 76344, Eggenstein-Leopoldshafen, Germany. ²Institute of Nanotechnology, Karlsruhe Institute of Technology (KIT), Hermann-von-Helmholtz-Platz 1, 76344, Eggenstein-Leopoldshafen, Germany. ³Karlsruhe Nano Micro Facility, Karlsruhe Institute of Technology (KIT), Hermann-von-Helmholtz-Platz 1, 76344, Eggenstein-Leopoldshafen, Germany. ⁴Institute of Solid State Physics, Russian Academy of Sciences, Ac. Ossipyan str. 2, 142432, Chernogolovka, Russia. ⁵BASF SE, Carl-Bosch-Straße 38, 67056, Ludwigshafen, Germany. ⁶Institute of Physical Chemistry & Center for Materials Science, Justus-Liebig-University Giessen, Heinrich-Buff-Ring 17, 35392, Giessen, Germany. Correspondence and requests for materials should be addressed to S.N. (email: sven.neudeck@kit.edu) or T.B. (email: torsten.brezesinski@kit.edu)

LCO^{19,21,22,28–33} and NCM523 (50% Ni)^{34,35}, among others. In so doing, all electrode constituents (CAM, carbon black additive, polymer binder etc.) are covered by a coating and, thus, the entire accessible surface is protected from exposure to the electrolyte solution³⁶. Because the contact points between the CAM secondary particles, the conductive carbon black and the current collector remain free of ALD material, superior electron and lithium-ion transport properties can be expected for coated electrodes over powder^{19,22}. In addition, different processes and deposition conditions can be readily tested without time- and material-consuming preparation steps in between.

Despite the wide use of Al₂O₃ coatings in LIBs, a solid understanding of how and why they enhance the cycling performance has not yet been established. Several studies reported on reduced transition-metal dissolution after cycling and/or in storage^{18,20,22,36}. However, Jung *et al.* have shown that, for NCM523, transition-metal dissolution is not the main source of degradation, even at high cell voltages (up to 4.8 V vs. Li⁺/Li)³⁷. In agreement with the hypothesis of reduced transition-metal dissolution, lower HF concentrations in the electrolyte were observed for cells using Al₂O₃-coated cathodes^{6,18}. This indicates that aluminum oxide-based surface shells undergo reaction with detrimental HF. In fact, time-of-flight secondary ion mass spectrometry revealed the formation of AlF₃ and the corresponding AlO_xF_y intermediate(s), which has been described as a kind of “HF (or H₂O) scavenging” in the literature^{6,18,38}. Nevertheless, studies on NCM523/Li cells cycled in the voltage range between 3.0 and 4.5 V reported the presence of Al₂O₃ after 100 cycles³⁴, with no indication of the formation of fluorine species after 40 cycles⁸. Regardless of composition, an Al-containing layer was found on the CAM surface after cycling^{24,38}, which, in some cases, appeared to be thinner than before^{34,36}.

Because of the transition-metal dissolution, changes in CAM surface composition and morphology are apparently inevitable. However, Al₂O₃ coatings were reported to reduce or even prevent corrosion^{6,24,38}. Furthermore, some studies concluded that irreversible transformations from layered to spinel^{24,25} and/or rock-salt-like phases^{9,34} at the CAM surface are inhibited by the presence of Al₂O₃. According to Jung *et al.* and Li *et al.*, the formation of a detrimental surface layer in pristine NCM523 and NCM811, respectively, depends upon the upper cutoff voltage during cycling operation^{37,39}.

So far, only few studies reported on the coating of technologically important CAMs such as Ni-rich NCM²⁴. Besides, half-cells with a lithium-metal anode are usually tested and often only for a limited number of cycles at relatively harsh conditions (i.e., high temperature and/or cutoff voltage). The processes and phenomena observed in such experiments are not necessarily reflecting those prevailing in real-world applications. Overall, there is clearly a lack of long-term performance studies of graphite-based full-cells using ALD-modified CAM under reasonable cycling conditions.

Here, we applied the strategy of Al₂O₃ ALD to practical NCM622 (60% Ni) cathodes and examined their performance in LIB full-cells over hundreds of cycles. The leaching of transition-metal species from the CAM or, more rigorously, their deposition at the graphite anode and changes in bulk and surface structure were investigated by a combination of *operando* X-ray diffraction (XRD), inductively coupled plasma-optical emission spectroscopy (ICP-OES) and advanced electron microscopy.

Results

Electrode Preparation and Characterization. NCM622 composite cathodes were coated with Al₂O₃ using 4, 10 and 40 ALD growth cycles (referred to as ALD-4@NCM622, ALD-10@NCM622 and ALD-40@NCM622, respectively, hereafter). The deposition temperature was set to 110 °C to avoid thermal damage to the electrodes. The final ALD precursor exposure was always TMA. The reason is the detrimental effect of residual H₂O and surface OH-groups on the cycling performance of LIB cells⁴⁰. According to established growth-per-cycle data (~0.13 nm between 100 and 125 °C on Si substrate)⁴¹, the Al₂O₃ layer thickness was estimated to about 0.5, 1.3 and 5.3 nm for ALD-4@NCM622, ALD-10@NCM622 and ALD-40@NCM622, respectively.

ALD-40@NCM622 was used as a model material to ensure the ALD was successful and, more importantly, to determine whether the coating was homogeneous throughout the bulk of the cathode. Cross-sectional focused ion beam (FIB)-scanning electron microscopy (SEM) imaging and energy-dispersive X-ray spectroscopy (EDX) provided clear evidence of the presence of Al in the interior of electrodes (Supplementary Fig. 1). From this data, it appears that the material was primarily deposited on the surface of CAM secondary particles. Given that the total Al content is very low, even for ALD-40@NCM622, proper characterization of the Al₂O₃ coating required much higher spatial resolution. Thus, transmission electron microscopy (TEM) was conducted on the ALD-10@NCM622, as the surface shell of ALD-40@NCM622 is too thick for any practical use in LIBs.

Both bright-field (BF)-TEM and Z-sensitive high-angle annular dark-field (HAADF)-scanning TEM (STEM) revealed the presence of a thin, amorphous layer on the top surface of secondary particles (Fig. 1 and Supplementary Fig. 2). The NCM622 CAM was rather uniformly covered with the layer thickness varying from 1 to 4 nm on flat parts of the surface. However, in areas where the surface is uneven, and especially at the contact points of particles, the coating was much thicker, even reaching a thickness of >10 nm. Such deviations from the expected value based on reported growth-per-cycle data were also observed for other substrates with “non-ideal” surfaces^{21,42,43}, and explained by additional hydrogen-bonded H₂O on the hydroxylated Al₂O₃, leading to a faster growth rate. Furthermore, it should be noted that the electrode itself may contain residual H₂O from the preparation process, which readily reacts with the TMA precursor.

TEM-EDX mapping also corroborated the presence of an Al-based surface layer in the case of ALD-10@NCM622 (Fig. 2 and Supplementary Fig. 3). Because the Pt-M and Al-K lines are very close together, the default procedure for map extraction produced strongly overlapping signals. To distinguish between the two elements, the Al map was extracted using a narrow energy window at the signal position in the EDX spectrum.

Cycling Performance. The electrochemical performance of the NCM622 CAM before and after Al₂O₃ ALD was evaluated at 25 °C in coin cells with both lithium-metal and graphite anodes. The initial specific discharge capacity at 0.1C of ALD-10@NCM622 half-cells [(166.7 ± 0.4) mAh/g_{NCM}] was found to be slightly lower than

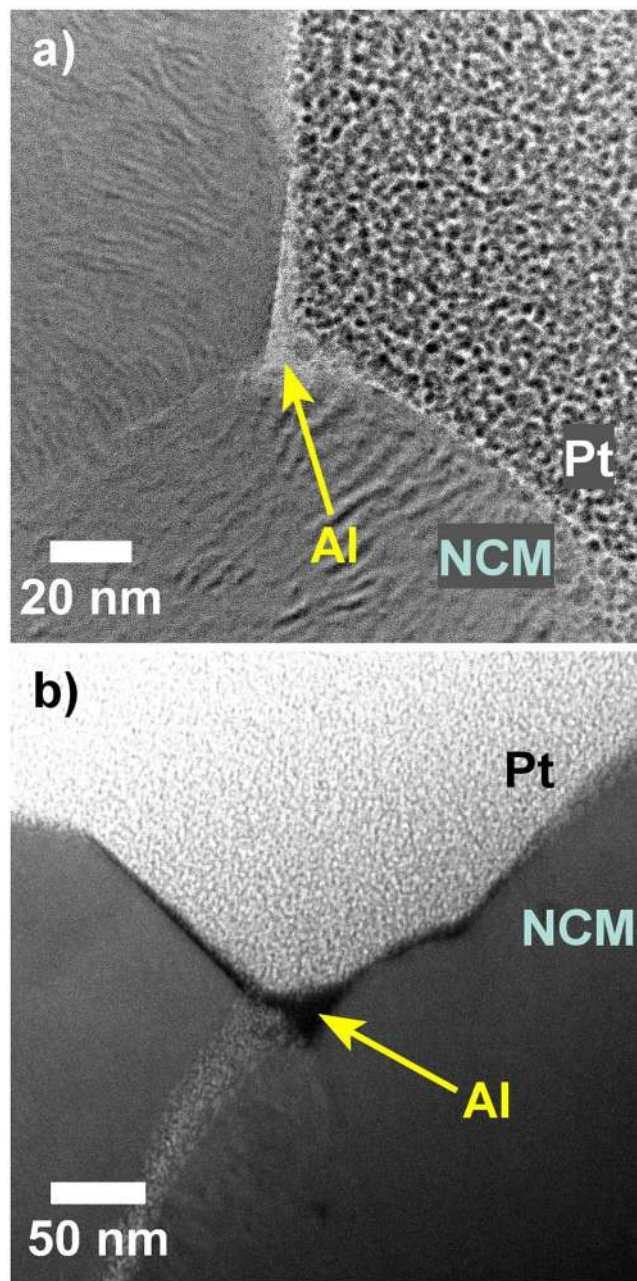


Figure 1. (a) BF-TEM and (b) HAADF-STEM images of ALD-10@NCM622. The electrode used was covered by a platinum (Pt) layer to protect the Al_2O_3 coating from damage during sample preparation and processing.

that of both ALD-4@NCM622 [$(167.5 \pm 0.2) \text{ mAh/g}_{\text{NCM}}$] and bare NCM622 [$(167.9 \pm 0.3) \text{ mAh/g}_{\text{NCM}}$]. This result indicates that about $1 \text{ mAh/g}_{\text{NCM}}$ of discharge capacity is lost due to surface coating when using 10 ALD growth cycles. Part of the reason is the lower active material content.

The mass of ALD-derived Al_2O_3 can be estimated assuming that the difference in discharge capacity is only due to differences in CAM content. When further considering the specific surface area of the bare NCM622 from gas adsorption ($0.47 \text{ m}^2/\text{g}_{\text{NCM}}$) and the solid-state density of Al_2O_3 (3.97 g/cm^3)⁴⁴, the average shell thickness can be calculated as 4 nm for ALD-10@NCM622, which agrees with the TEM results. Besides, it should be noted that the difference in discharge capacity can probably also be attributed to lithiation of the Al_2O_3 layer^{45,46}.

The rate capability was tested by charging the half-cells at 0.25C and discharging them at rates ranging from 0.1 to 3C (Supplementary Fig. 4). Hardly any differences in specific discharge capacity within the experimental error were observed between ALD-4@NCM622 and bare NCM622, whereas the cells using ALD-10@NCM622 delivered overall lower capacities, especially at rates $\geq 1\text{C}$, thus indicating that the thicker Al_2O_3 coating somewhat hinders charge transfer. Furthermore, the data demonstrate that the ALD-coated NCM622 CAMs are capable of outperforming the reference material in terms of capacity retention. After 100 cycles, both the ALD-10@NCM622 and ALD-4@NCM622 cells delivered discharge capacities higher by about $2 \text{ mAh/g}_{\text{NCM}}$ than the bare

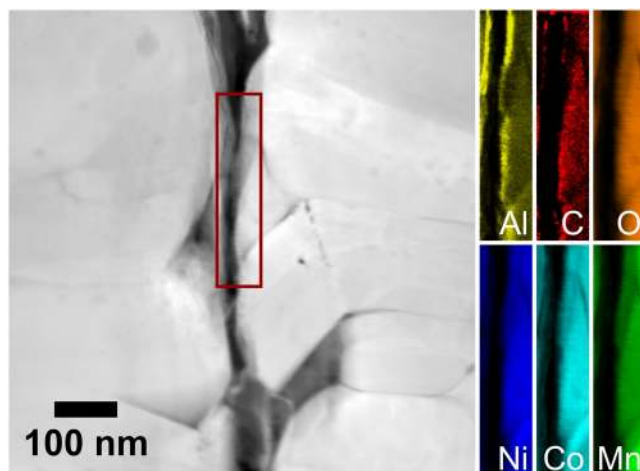


Figure 2. HAADF-STEM image of ALD-10@NCM622 and the corresponding EDX maps for the area between two adjacent CAM secondary particles denoted by the red box.

NCM622. In summary, we conclude that, regardless of thickness, Al_2O_3 coating on NCM622 composite cathodes leads to improved capacity retention. However, a relatively thicker surface shell results in lower initial discharge capacity and rate capability. Thus, in terms of absolute capacity and kinetics, the ALD layer should be as thin as possible.

The graphite-based full-cells were cycled at a rate of 1C in the voltage range between 2.8 and 4.2 V with a constant voltage (CV) step at the upper cutoff voltage. A rate capability test was implemented every 100 cycles. Figure 3 and Supplementary Fig. 5 depict cycling data averaged from at least 4 independent experiments (cells), thereby allowing for fair comparison, especially of the ALD-coated NCM622 CAMs. As expected, all cells delivered similar initial discharge capacities of (164 ± 1) mAh/g_{NCM} at 0.1C. At 1C rate, the discharge capacity of both the ALD-4@NCM622 and ALD-10@NCM622 cells was found to be slightly lower for the first 200 to 300 cycles (Supplementary Fig. 5). The capacity decay in the subsequent cycles was almost linear for the different CAMs employed in this work. As for capacity retention, ALD-4@NCM622 and ALD-10@NCM622 clearly outperformed the bare NCM622 (Fig. 3a). After 1400 cycles, the ALD-10@NCM622 cells still delivered a specific discharge capacity of (127.2 ± 0.6) mAh/g_{NCM}, corresponding to $(84.8 \pm 0.4)\%$ relative to the 5th cycle capacity at 1C. While similar results were obtained for ALD-4@NCM622 [(126.5 ± 0.4) mAh/g_{NCM}, $(85.3 \pm 0.4)\%$], the performance of the bare NCM622 reference was considerably worse [(123.3 ± 0.2) mAh/g_{NCM}, $(81.6 \pm 0.2)\%$].

To better illustrate the improvement in longevity achieved by Al_2O_3 ALD coating, the cycle numbers, at which the cell capacity faded to 85% of its rated value, were compared. In fact, this was found to occur much earlier for bare NCM622, after 1069 cycles, compared to 1381 cycles for ALD-10@NCM622. Considering the capacity decay rates, the difference in cycle number between the cells is projected to be even larger for 80% capacity retention, which is typically defined as end-of-life of commercial battery cells⁴⁷.

The Coulombic efficiency of all cells increased to $> 99.95\%$ within the first 20 cycles (Fig. 3b). As anticipated based on the above data, the Coulombic efficiency of the bare NCM622 cells was slightly lower than that of cells using the ALD-coated CAMs over the entire 1400 cycles. The cell impedance reflected the same trend. During the first 70 cycles, both the ALD-4@NCM622 and ALD-10@NCM622 cells exhibited a higher resistance, expressed by higher mean charge voltages (Fig. 3c). This is clearly due to the presence of Al_2O_3 coating on the composite cathodes, which apparently raises the energy barrier for (ionic) charge transfer. However, a much stronger increase in mean charge voltage with prolonged cycling was observed for the bare NCM622. Again, there was no significant difference between the ALD-4@NCM622 and ALD-10@NCM622 cells. Other measures of cell resistance such as mean discharge voltage and specific capacity gained in the CV step during charging revealed similar trends (Supplementary Fig. 5).

The effect of Al_2O_3 ALD on the kinetics was also somewhat reflected in the capacity retention data (see temporary capacity decline right after rate performance testing during cycling). Furthermore, the rate capability results agreed with the trends seen in cycling performance and impedance buildup (Fig. 3d and Supplementary Fig. 6). During the first test after around 10 cycles, the extent of capacity decrease at rates $\geq 2\text{C}$ was found to be slightly lower for bare NCM622 than the ALD-coated CAMs. At 3C, the specific discharge capacity of the bare NCM622 cells was lower by (20.5 ± 0.4) mAh/g_{NCM} relative to that delivered at 0.5C rate [(23.0 ± 0.4) mAh/g_{NCM} for ALD-4@NCM622 and (22.6 ± 0.5) mAh/g_{NCM} for ALD-10@NCM622]. However, this trend was reversed after 200 cycles (e.g., $[41 \pm 2]$ mAh/g_{NCM} for bare NCM622, compared to $[30.5 \pm 0.8]$ mAh/g_{NCM} for ALD-4@NCM622 and $[29.3 \pm 0.8]$ mAh/g_{NCM} for ALD-10@NCM622 at 3C rate after around 1300 cycles; see Fig. 3d).

The data discussed thus far clearly establish that Al_2O_3 ALD coating of NCM622 composite cathodes brings about significant improvements in stability and cycling performance of LIB full-cells. Initially higher resistances and slower kinetics are quickly compensated for by a much weaker tendency for impedance buildup compared to the bare NCM622 cells. Note that the number of ALD growth cycles (when ≥ 4 and ≤ 10) apparently does not play a major role in controlling the cyclability.

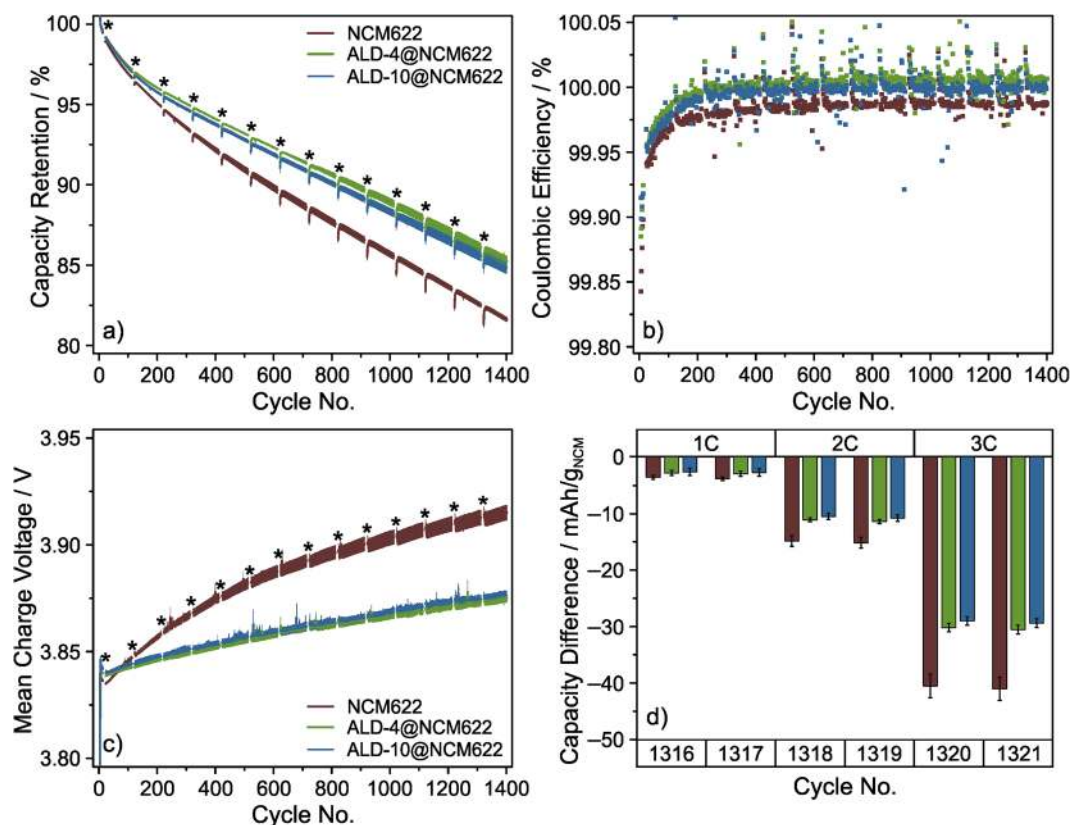


Figure 3. (a) Capacity retention relative to 5th cycle discharge capacity at 1C rate, (b) Coulombic efficiency and (c) mean charge voltage versus cycle number as well as (d) rate capability in the later cycles of graphite-based full-cells using bare NCM622, ALD-4@NCM622 and ALD-10@NCM622. After the initial formation cycles at 0.1C were completed, the cells were charged and discharged at 1C, with a rate performance test every 100 cycles (denoted by asterisks in (a,c); data omitted for clarity), during which they were charged at 0.5C and discharged at rates up to 3C. Differences in specific discharge capacity relative to that at 0.5C are shown in (d). Cycling results are averaged from several cells, with the error bars indicating the standard deviation of the mean.

Analysis of Failure Modes. To understand how ALD coating contributes to the performance improvement, electrodes harvested from cells after cycling for 1400 cycles were investigated by ICP-OES, *operando* XRD and TEM. Transition-metal leaching from the CAM particles is often claimed to be responsible (to some extent) for the capacity decay^{48,49}. In addition to loss of CAM, especially loss of active lithium, which is consumed during rebuilding of the graphite solid electrolyte interphase (SEI) due to continuous destruction/poisoning, needs to be considered^{50,51}. The amount of transition-metal species deposited at the anode side was determined via ICP-OES (Supplementary Fig. 7). Interestingly, the proportion of Mn was similar to that of Ni (about 0.6 mg/g_{graphite}), which is certainly due in part to the higher dissolution rate of Mn than both Co and Ni. However, the total amount is too small to explain the observed capacity losses. Most importantly, there were no significant differences between the cells. Consequently, transition-metal dissolution and subsequent deposition are unlikely to be the main reason for the different capacity fade rates. This result is in agreement with data reported for NCM523³⁷. It should be noted though that the type of separator used can greatly affect the transition-metal leaching by reacting with HF present in the electrolyte). Likewise, *operando* XRD did not indicate major differences with respect to bulk composition and crystallinity between the ALD-10@NCM622 and bare NCM622. The changes in *a* and *c* lattice parameters and, thus, also of unit cell volume upon Li insertion/extraction into/from the NCM lattice follow the trends observed in recent studies on Ni-rich NCMs and are more or less identical for both CAMs (Supplementary Fig. 8)^{52–57}.

Finally, the electrodes were characterized using TEM. Notably, even after cycling in full-cell configuration for 1400 cycles, an Al-containing surface layer was present on the ALD-10@NCM622 as evidenced by high-resolution (HR-)TEM and HAADF-STEM (Fig. 4). This result was further confirmed by TEM-EDX mapping (Supplementary Fig. 9). Although Al₂O₃ coating is widely used in the LIB area, only a limited number of studies reported experimental data on the robustness of the surface shell^{6,24,34,38}. Unfortunately, Al₂O₃ and AlF₃, the latter of which is believed to form by reaction with HF during cycling operation^{6,18,38}, could not be distinguished by EDX analysis. The reason is that the F-K line and the Co-L and Mn-L series are close together and background subtraction in this energy range is difficult. Thus, it remains unclear whether or not Al₂O₃ acted as an “HF scavenger” in the present work.

Direct comparison of the ALD-coated and bare NCM622 CAMs cycled under identical conditions revealed distinct differences in surface morphology (Fig. 5). The reference material appeared to be corroded to a much

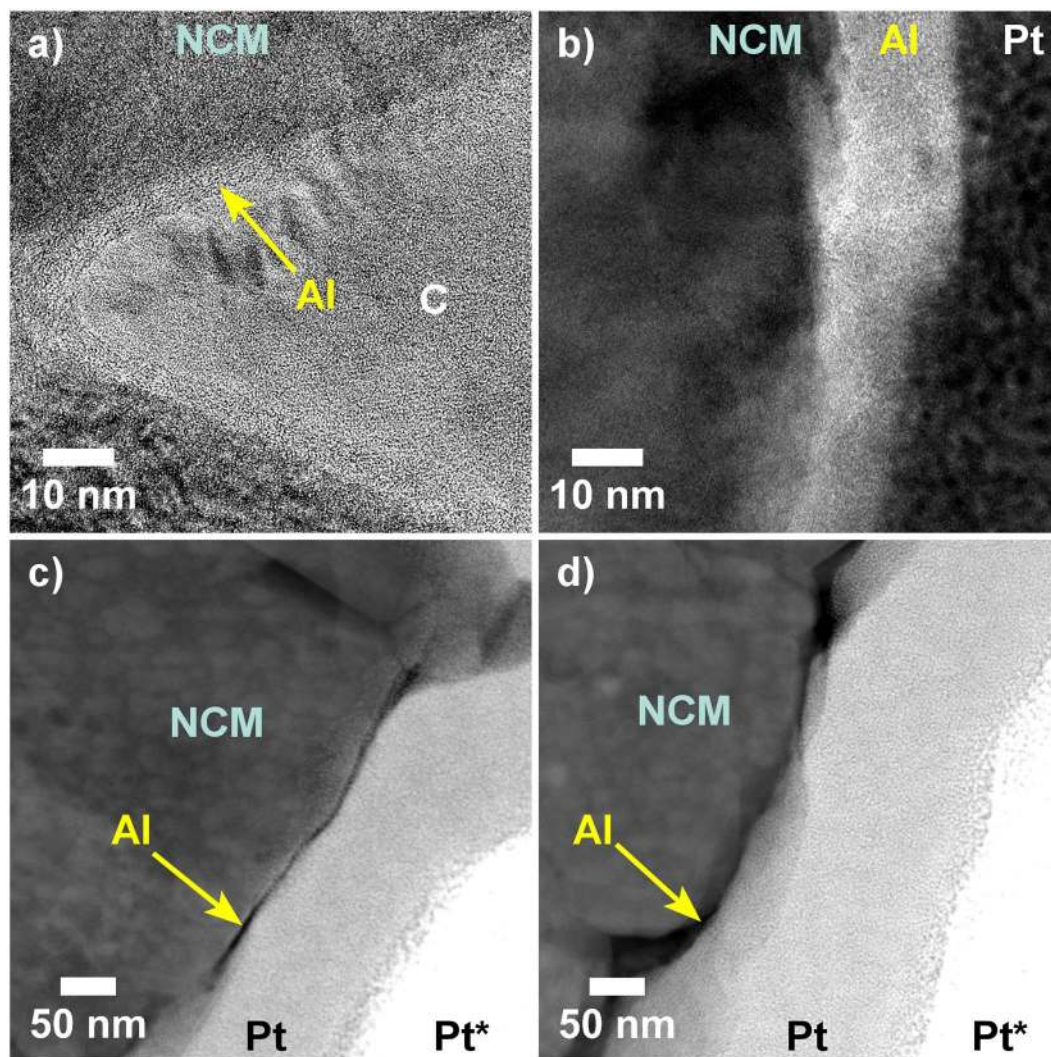


Figure 4. (a,b) HR-TEM and (c,d) HAADF-STEM images of ALD-10@NCM622 after cycling in full-cell configuration for 1400 cycles. The electrodes used were covered by carbon (C) or platinum protective layers, the latter of which were produced by electron-beam (Pt) and ion-beam (Pt*) assisted deposition.

greater extent. The ALD-10@NCM622 top surface was relatively smooth with uniform primary particles. In the case of bare NCM622, the presence of particles of much smaller size than the primary particles and without the typical radial orientation was observed. According to TEM-EDX mapping, these particles are made of transition-metal oxides (Supplementary Figs 10 and 11). However, as revealed by HAADF-STEM, lighter elements, probably arising from decomposition of the electrolyte solvents and the supporting salt, fill much of the intergranular space between them. In fact, both carbon and phosphorus were detected by EDX. Apparently, the NCM622 CAM is partially dissolved during the corrosion process and the empty space is filled with decomposition products from side reactions. Reprecipitation of solutes cannot be ruled out and might help explain the formation of smaller particles. This kind of corrosion was observed in many areas on the surface of bare NCM622 secondary particles as indicated by BF-STEM and HAADF-STEM measurements (Fig. 6 and Supplementary Figs 12 and 13). Both detachment of CAM and probably also of carbon black additive and polymer binder from the secondary particles and formation of a cathode SEI lead to loss of electrochemical activity and, therefore, capacity degradation.

Lastly, we note that close inspection of fast Fourier transform patterns of HR-TEM images did not indicate the presence of rock-salt-like phases. In addition, electron energy-loss spectroscopy core-loss spectra of transition-metal-L edges obtained on the ALD-10@NCM622 at different areas of the primary particles did not reveal signs of chemical shifts, which may be expected for a layered-to-rock-salt transformation^{58,59}. However, as mentioned previously^{37,39}, the formation of rock-salt structure on the surface of Ni-rich NCM CAMs apparently depends on the cutoff voltage in the charge cycle and may be inhibited or even prevented by the presence of Al₂O₃ surface shells. Nevertheless, this needs further study.

We emphasize once again that the general cycling conditions (separator type, volume of electrolyte in the cell, cutoff voltage etc.) have a profound effect on the degradation processes occurring in LIB cells. For example, the

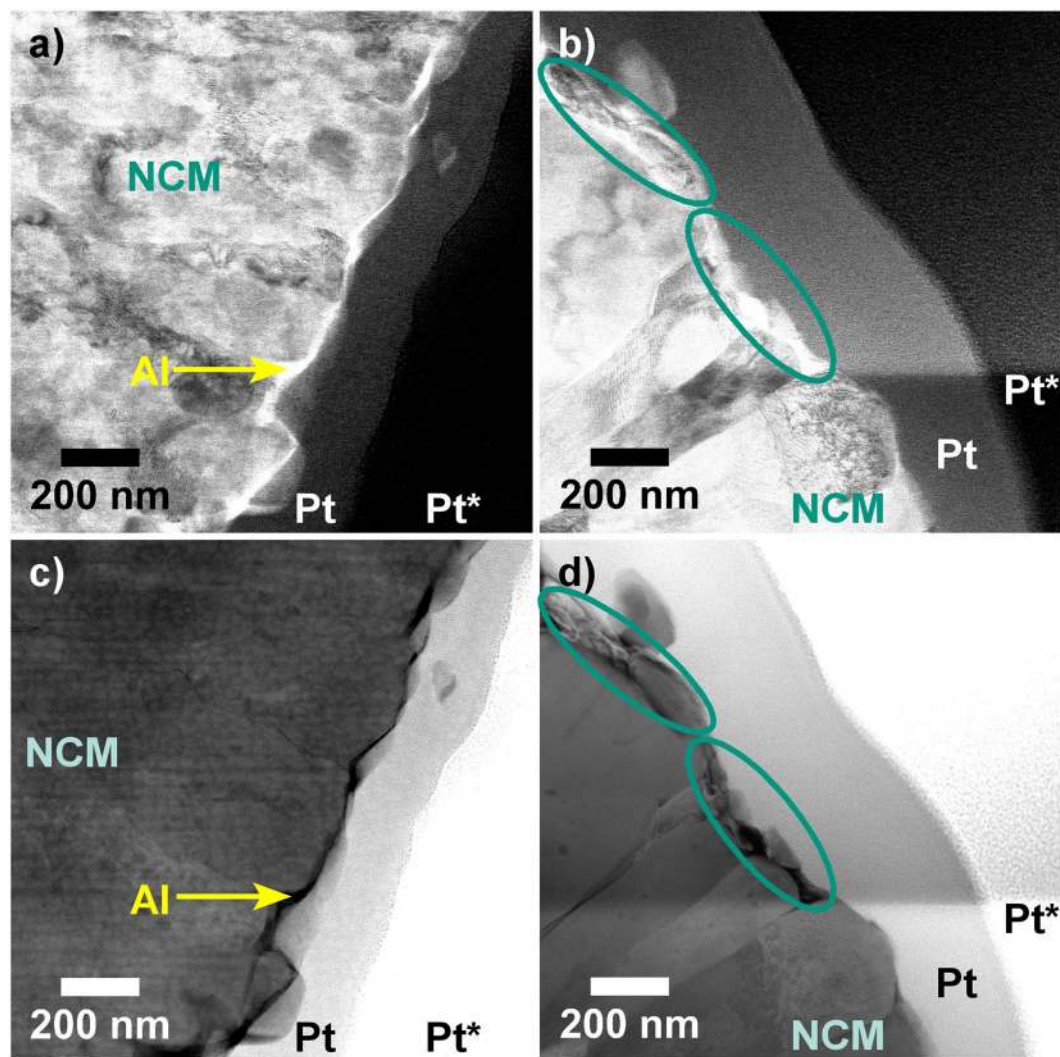


Figure 5. (a,b) BF-STEM and (c,d) HAADF-STEM images of ALD-10@NCM622 (a,c) and bare NCM622 (b,d) after cycling in full-cell configuration for 1400 cycles. Areas of pronounced surface degradation are denoted by green ellipses. The electrodes used were covered by platinum protective layers, produced by electron-beam (Pt) and ion-beam (Pt*) assisted deposition.

glass fiber separator used here can potentially react with the HF in the electrolyte, thus indirectly affecting the cell chemistry. By rigorously comparing different materials under identical conditions, as done in this study, we identified the surface corrosion as being a major cause of degradation in the case of uncoated NCM622. Other mechanisms, triggered by particle fracture, transition-metal deposition on the anode or formation of rock-salt-like phases on the CAM particle surface, to name a few, may come into play under different conditions. Thus, further work is clearly necessary to fully understand the specific degradation pathways and the role of thin surface coatings in the battery area.

Discussion

NCM622 composite cathodes of practical loading were successfully coated by Al_2O_3 ALD. The coating thickness was controlled by varying the number of ALD growth cycles. Characterization of the modified cathodes via electron microscopy and X-ray spectroscopy revealed that Al_2O_3 , which appears to be primarily deposited on the surface of secondary particles, is present throughout the bulk of the electrode.

Electrochemical testing was performed in half- and full-cells. The Al_2O_3 -coated NCM622 clearly outperformed the uncoated reference material in terms of capacity retention and efficiency (e.g., much lower cell impedance growth with cycling), even under moderate conditions. In graphite-based cells, the number of ALD growth cycles when ≥ 4 and ≤ 10 was found to not play a major role in controlling the performance and rate capability. Transmission electron microscopy studies comparing the coated and uncoated NCM622 demonstrated that the Al_2O_3 surface shell is well preserved after cycling in full-cell configuration for 1400 cycles and, even more importantly, effectively reduces corrosion. Only the top surface of ALD-coated NCM622 appeared smooth and largely intact, correlating with the observed cycling performance and helping to explain the improved longevity.

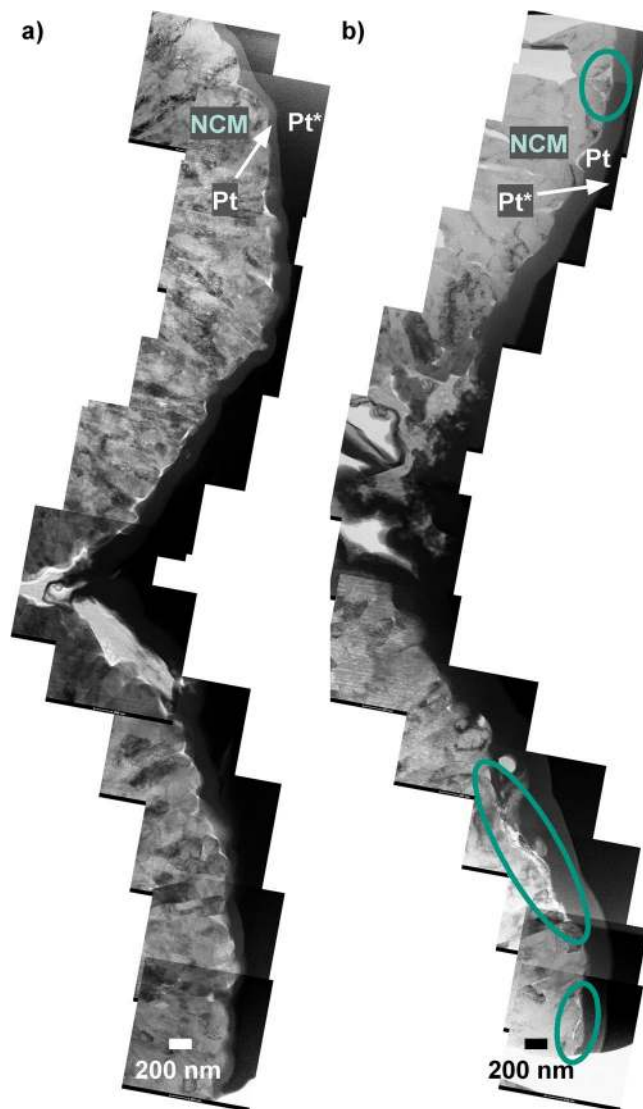


Figure 6. BF-STEM images of ALD-10@NCM622 (a) and bare NCM622 (b) after cycling in full-cell configuration for 1400 cycles. The top surface of two adjacent secondary particles is reconstructed by stringing together overlapping images. Areas of pronounced surface degradation are denoted by green ellipses. The electrodes used were covered by platinum protective layers, produced by electron-beam (Pt) and ion-beam (Pt*) assisted deposition. Corresponding HAADF-STEM images are shown in Supplementary Fig. 13.

There were hardly any differences in bulk lattice structure and transition-metal leaching between the coated and uncoated NCM622. Furthermore, no clear evidence of surface phase transformations for a charging voltage of 4.2 V vs. graphite was found. Taken together, our data establish that the cathode-electrolyte interphase stability is greatly enhanced by Al_2O_3 ALD.

Methods

Electrode Preparation. Solef5130 polyvinylidene fluoride (PVDF) binder was dissolved in *N*-methyl-2-pyrrolidone (NMP, Merck; Germany) to prepare a 7.5 wt.% solution. For the preparation of electrodes, binder (3 wt.%) solution, SFG6L graphite (2 wt.%) and Super C65 carbon black (1 wt.%) were suspended in NMP. After mixing for 3 min at 2000 rpm and then for another 3 min at 400 rpm using an ARE 250 planetary centrifugal mixer (Thinky Corp.; Japan), NCM622 CAM (94 wt.%, BASF SE; Germany) was added. The suspension was mixed twice at the above conditions to obtain the final slurry. The solid content was adjusted to 65% by addition of extra NMP during mixing in the first place. The slurry was coated onto aluminum foil using a doctor blade on a film applicator (Coatmaster 510, Erichsen GmbH & Co. KG; Germany). After drying in vacuum at 120 °C (VDL 53, Binder GmbH; Germany), the cathodes were calendared at 10 N/mm using a laboratory calendar (Sumet Systems GmbH; Germany). The areal loading was 11.6–11.7 $\text{mg}_{\text{NCM}}/\text{cm}^2$.

ALD Coating. Al_2O_3 ALD on NCM622 composite cathodes was performed on a SUNALE R-200 Advanced (Picosun; Finland). The electrodes were mounted on an 8'' Si(001) wafer and then heated to 110 °C. The two

half-reaction steps consisted of injecting five times TMA or H₂O with 0.1 s purging between each pulse and purging of 40 s after the last pulse. 4, 10 and 40 ALD growth cycles were used to prepare the Al₂O₃-coated cathodes.

Cell Assembly. CR2032 coin cells (Hohsen Corp.; Japan) were assembled inside an argon-filled glovebox (MBraun; Germany) using materials pre-dried at 100 °C in vacuum. For half-cells, NCM622 cathode (Ø14 mm), lithium-metal anode (Ø15 mm, Gelon LIB Co.; China) and glass fiber separator (GF/D Whatman, GE Healthcare Life Sciences; USA) soaked with electrolyte solution (200 µL LP47 [1.0 M LiPF₆ in 3:7 by weight ethylene carbonate (EC)/diethyl carbonate (DEC)], BASF SE; Germany) were used.

Full-cells were assembled using NCM622 cathode (Ø14 mm), graphite anode (Ø15 mm, 6.8 mg_{graphite}/cm², BASF SE; Germany) and glass fiber separator (GF/A Whatman) soaked with electrolyte solution (100 µL LP472 [LP47 containing 2 wt.% vinylene carbonate], BASF SE; Germany). All cells were sealed using an MSK-160D crimper (MTI Corp.; USA).

Cell Disassembly. Discharged cells were de-crimped inside the glovebox. The cathode was harvested and rinsed with DEC (4 × 250 µL, Sigma-Aldrich; Germany). After soaking in DEC (500 µL), the separator and graphite anode were carefully separated and the latter was washed with DEC (2 × 250 µL).

Cell Testing. Electrochemical testing was performed at 25 °C on a Series 4000 multichannel battery cycler (MACCOR Inc.; USA). After equilibration for 2 h, half-cells were cycled between 3.0 and 4.3 V with a constant voltage (CV) step at the upper cutoff voltage, followed by a 5 min resting period prior to discharge. During the initial three cycles at 0.1C (1C = 160 mA/g_{NCM}), the CV step was limited either by time (30 min) or by residual current (0.01C). The cells were then charged at 0.25C, with the CV step limited to 20 min or 0.05C, and discharged at different rates from 0.1 to 3C for three cycles each. Eventually, the discharge rate was set to 0.5C. Half-cell data are averaged from two (for ALD-4@NCM622) and three independent cells (for bare NCM622 and ALD-10@NCM622).

After equilibration for 6 h, full-cells were cycled between 2.8 and 4.2 V with a CV step at 4.2 V. The CV step was also limited by time (1 h) or residual current (0.02C), followed by a 5 min resting period. After three formation cycles at 0.1C were completed, the cells were cycled at 1C, with a rate performance test every 100 cycles (charging at 0.5C and discharging at different rates of 0.5, 1, 2 and 3C for two consecutive cycles). Long-term cycling data are averaged from four (for ALD-4@NCM622 and ALD-10@NCM622) and seven independent cells (for bare NCM622).

Instrumentation. The content of transition-metal species in/on the graphite anode after cycling was determined by ICP-OES using both a PerkinElmer Optima 4300 DV and a Thermo Scientific iCAP 7600. ICP-OES data are averaged from three independent cells. FIB-SEM-EDX was performed on a ZEISS Auriga 60. TEM was performed on both FEI Tecnai F20 and TITAN 60–300 microscopes. To protect the Al₂O₃ coating from damage during sample preparation and later processing, the specimens were covered by a layer of carbon and/or platinum produced by initial electron-beam and subsequent ion-beam assisted deposition using an FEI Strata Dual Beam instrument. After formation of the protective layer(s), TEM specimens were prepared by gallium focused ion-beam milling. XRD was performed in transmission mode (300 s exposure time) on a custom Mo-K_{α1,2} diffractometer. The intensity of two consecutive 2D patterns was added up and integrated, yielding high-quality 1D data for analysis.

Data Availability

All data generated or analyzed during this study are included in this published article (and its Supplementary Information files).

References

- Myung, S.-T. *et al.* Nickel-rich layered cathode materials for automotive lithium-ion batteries: Achievements and perspectives. *ACS Energy Lett.* **2**, 196–223 (2017).
- Blomgren, G. E. The development and future of lithium ion batteries. *J. Electrochem. Soc.* **164**, A5019–A5025 (2017).
- Kim, J. *et al.* Prospect and reality of Ni-rich cathode for commercialization. *Adv. Energy Mater.* **8**, 1702028 (2018).
- Radin, M. D. *et al.* Narrowing the gap between theoretical and practical capacities in Li-ion layered oxide cathode materials. *Adv. Energy Mater.* **7**, 1602888 (2017).
- Neudeck, S. *et al.* Molecular surface modification of NCM622 cathode material using organophosphates for improved Li-ion battery full-cells. *ACS Appl. Mater. Interfaces* **10**, 20487–20498 (2018).
- Myung, S.-T. *et al.* Role of alumina coating on Li–Ni–Co–Mn–O particles as positive electrode material for lithium-ion batteries. *Chem. Mater.* **17**, 3695–3704 (2005).
- Taguchi, N., Akita, T., Sakaebe, H., Tatsumi, K. & Ogumi, Z. Characterization of the surface of LiCoO₂ particles modified by Al and Si oxide using analytical TEM. *J. Electrochem. Soc.* **160**, A2293–A2298 (2013).
- Han, B. *et al.* Understanding the role of temperature and cathode composition on interface and bulk: Optimizing aluminum oxide coatings for Li-ion cathodes. *ACS Appl. Mater. Interfaces* **9**, 14769–14778 (2017).
- Yano, A. *et al.* Surface structure and high-voltage charge/discharge characteristics of Al-oxide coated LiNi_{1/3}Co_{1/3}Mn_{1/3}O₂ cathodes. *J. Electrochem. Soc.* **162**, A3137–A3144 (2015).
- Neudeck, S. *et al.* Room temperature, liquid-phase Al₂O₃ surface coating approach for Ni-rich layered oxide cathode material. *Chem. Commun.* **55**, 2174–2177 (2019).
- Meng, X., Yang, X.-Q. & Sun, X. Emerging applications of atomic layer deposition for lithium-ion battery studies. *Adv. Mater.* **24**, 3589–3615 (2012).
- Ma, L. *et al.* Atomic layer deposition for lithium-based batteries. *Adv. Mater. Interfaces* **3**, 1600564 (2016).
- Kim, J. W. *et al.* Surface chemistry of LiNi_{0.5}Mn_{1.5}O₄ particles coated by Al₂O₃ using atomic layer deposition for lithium-ion batteries. *J. Power Sources* **274**, 1254–1262 (2015).
- Zhang, X. *et al.* Structural and electrochemical study of Al₂O₃ and TiO₂ coated Li_{1.2}Ni_{0.13}Mn_{0.54}Co_{0.13}O₂ cathode material using ALD. *Adv. Energy Mater.* **3**, 1299–1307 (2013).

15. Puurunen, R. L. Surface chemistry of atomic layer deposition: A case study for the trimethylaluminum/water process. *J. Appl. Phys.* **97**, 121301 (2005).
16. George, S. M. Atomic layer deposition: An overview. *Chem. Rev.* **110**, 111–131 (2010).
17. Reitz, C. *et al.* Hierarchical carbon with high nitrogen doping level: A versatile anode and cathode host material for long-life lithium-ion and lithium–sulfur batteries. *ACS Appl. Mater. Interfaces* **8**, 10274–10282 (2016).
18. Oh, Y., Ahn, D., Nam, S. & Park, B. The effect of Al₂O₃-coating coverage on the electrochemical properties in LiCoO₂ thin films. *J. Solid State Electrochem.* **14**, 1235–1240 (2009).
19. Jung, Y. S. *et al.* Ultrathin direct atomic layer deposition on composite electrodes for highly durable and safe Li-ion batteries. *Adv. Mater.* **22**, 2172–2176 (2010).
20. Kim, Y. J., Cho, J., Kim, T.-J. & Park, B. Suppression of cobalt dissolution from the LiCoO₂ cathodes with various metal-oxide coatings. *J. Electrochem. Soc.* **150**, A1723–A1725 (2003).
21. Jung, Y. S. *et al.* Enhanced stability of LiCoO₂ cathodes in lithium-ion batteries using surface modification by atomic layer deposition. *J. Electrochem. Soc.* **157**, A75–A81 (2010).
22. Li, X. *et al.* Significant impact on cathode performance of lithium-ion batteries by precisely controlled metal oxide nanocoatings via atomic layer deposition. *J. Power Sources* **247**, 57–69 (2014).
23. Riley, L. A. *et al.* Electrochemical effects of ALD surface modification on combustion synthesized LiNi_{1/3}Mn_{1/3}Co_{1/3}O₂ as a layered-cathode material. *J. Power Sources* **196**, 3317–3324 (2011).
24. Mohanty, D. *et al.* Modification of Ni-rich FCG NMC and NCA cathodes by atomic layer deposition: Preventing surface phase transitions for high-voltage lithium-ion batteries. *Sci. Rep.* **6**, 26532 (2016).
25. Kim, J. W. *et al.* Unexpected high power performance of atomic layer deposition coated Li[Ni_{1/3}Mn_{1/3}Co_{1/3}]O₂ cathodes. *J. Power Sources* **254**, 190–197 (2014).
26. Fang, S., Jackson, D., Dreibelbis, M. L., Kuech, T. F. & Hamers, R. J. Anode-originated SEI migration contributes to formation of cathode-electrolyte interphase layer. *J. Power Sources* **373**, 184–192 (2018).
27. Jackson, D. H. & Kuech, T. F. Electrochemical effects of annealing on atomic layer deposited Al₂O₃ coatings on LiNi_{0.5}Mn_{0.3}Co_{0.2}O₂. *J. Power Sources* **365**, 61–67 (2017).
28. Scott, I. D. *et al.* Ultrathin coatings on nano-LiCoO₂ for Li-ion vehicular applications. *Nano Lett.* **11**, 414–418 (2011).
29. Jung, Y. S. *et al.* Unexpected improved performance of ALD coated LiCoO₂/graphite Li-ion batteries. *Adv. Energy Mater.* **3**, 213–219 (2013).
30. Lee, J.-T., Wang, F.-M., Cheng, C.-S., Li, C.-C. & Lin, C.-H. Low-temperature atomic layer deposited Al₂O₃ thin film on layer structure cathode for enhanced cycleability in lithium-ion batteries. *Electrochim. Acta* **55**, 4002–4006 (2010).
31. Cheng, H.-M. *et al.* Enhanced cycleability in lithium ion batteries: Resulting from atomic layer deposition of Al₂O₃ or TiO₂ on LiCoO₂ electrodes. *J. Phys. Chem. C* **116**, 7629–7637 (2012).
32. Xie, M., Li, B. & Zhou, Y. Free-standing high-voltage LiCoO₂/multi-wall carbon nanotube paper electrodes with extremely high areal mass loading for lithium ion batteries. *J. Mater. Chem. A* **3**, 23180–23184 (2015).
33. Xie, J. *et al.* Engineering the surface of LiCoO₂ electrodes using atomic layer deposition for stable high-voltage lithium ion batteries. *Nano Res.* **10**, 3754–3764 (2017).
34. Su, Y. *et al.* Enhancing the high-voltage cycling performance of LiNi_{0.5}Mn_{0.3}Co_{0.2}O₂ by retarding its interfacial reaction with an electrolyte by atomic-layer-deposited Al₂O₃. *ACS Appl. Mater. Interfaces* **7**, 25105–25112 (2015).
35. Shi, Y., Zhang, M., Qian, D. & Meng, Y. S. Ultrathin Al₂O₃ coatings for improved cycling performance and thermal stability of LiNi_{0.5}Co_{0.2}Mn_{0.3}O₂ cathode material. *Electrochim. Acta* **203**, 154–161 (2016).
36. Bettge, M. *et al.* Improving high-capacity Li_{1.2}Ni_{0.15}Mn_{0.55}Co_{0.1}O₂-based lithium-ion cells by modifying the positive electrode with alumina. *J. Power Sources* **233**, 346–357 (2013).
37. Jung, S.-K. *et al.* Understanding the degradation mechanisms of LiNi_{0.5}Co_{0.2}Mn_{0.3}O₂ cathode material in lithium ion batteries. *Adv. Energy Mater.* **4**, 1300787 (2014).
38. Myung, S.-T. *et al.* Functionality of oxide coating for Li[Li_{0.05}Ni_{0.4}Co_{0.15}Mn_{0.4}]O₂ as positive electrode materials for lithium-ion secondary batteries. *J. Phys. Chem. C* **111**, 4061–4067 (2007).
39. Li, J. *et al.* The impact of electrolyte additives and upper cut-off voltage on the formation of a rocksalt surface layer in LiNi_{0.8}Mn_{0.1}Co_{0.1}O₂ electrodes. *J. Electrochem. Soc.* **164**, A655–A665 (2017).
40. Metzger, M., Strehle, B., Solchenbach, S. & Gasteiger, H. A. Hydrolysis of ethylene carbonate with water and hydroxide under battery operating conditions. *J. Electrochem. Soc.* **163**, A1219–A1225 (2016).
41. Groner, M. D., Fabreguette, F. H., Elam, J. W. & George, S. M. Low-temperature Al₂O₃ atomic layer deposition. *Chem. Mater.* **16**, 639–645 (2004).
42. McCormick, J. A., Rice, K. P., Paul, D. F., Weimer, A. W. & George, S. M. Analysis of Al₂O₃ atomic layer deposition on ZrO₂ nanoparticles in a rotary reactor. *Chem. Vap. Deposition* **13**, 491–498 (2007).
43. Ferguson, J. D., Weimer, A. W. & George, S. M. Atomic layer deposition of Al₂O₃ films on polyethylene particles. *Chem. Mater.* **16**, 5602–5609 (2004).
44. Sporer, R. W., Landau, U., Kuo, H.-H. H. & Wang, Y.-M. A process for etching modulated profiles. *J. Electrochem. Soc.* **155**, D651–D659 (2008).
45. Jung, S. C. & Han, Y.-K. How do Li atoms pass through the Al₂O₃ coating layer during lithiation in Li-ion batteries? *J. Phys. Chem. Lett.* **4**, 2681–2685 (2013).
46. Liu, Y. *et al.* *In situ* transmission electron microscopy observation of pulverization of aluminum nanowires and evolution of the thin surface Al₂O₃ layers during lithiation–delithiation cycles. *Nano Lett.* **11**, 4188–4194 (2011).
47. Talaie, E. *et al.* Methods and protocols for electrochemical energy storage materials research. *Chem. Mater.* **29**, 90–105 (2017).
48. Zheng, H., Sun, Q., Liu, G., Song, X. & Battaglia, V. S. Correlation between dissolution behavior and electrochemical cycling performance for LiNi_{1/3}Co_{1/3}Mn_{1/3}O₂-based cells. *J. Power Sources* **207**, 134–140 (2012).
49. Amine, K. *et al.* Mechanism of capacity fade of MCMB/Li_{1.1}[Ni_{1/3}Mn_{1/3}Co_{1/3}]O₂ cell at elevated temperature and additives to improve its cycle life. *J. Mater. Chem.* **21**, 17754–17759 (2011).
50. Waldmann, T., Wilka, M., Kasper, M., Fleischhammer, M. & Wohlfahrt-Mehrens, M. Temperature dependent ageing mechanisms in lithium-ion batteries – A post-mortem study. *J. Power Sources* **262**, 129–135 (2014).
51. Zheng, H. *et al.* Quantitative characterization of the surface evolution for LiNi_{0.5}Co_{0.2}Mn_{0.3}O₂/graphite cell during long-term cycling. *ACS Appl. Mater. Interfaces* **9**, 12445–12452 (2017).
52. Strauss, F. *et al.* Impact of cathode material particle size on the capacity of bulk-type all-solid-state batteries. *ACS Energy Lett.* **3**, 992–996 (2018).
53. Noh, H.-J., Youn, S., Yoon, C. S. & Sun, Y.-K. Comparison of the structural and electrochemical properties of layered Li[Ni_xCo_yMn_z]O₂ (x = 1/3, 0.5, 0.6, 0.7, 0.8 and 0.85) cathode material for lithium-ion batteries. *J. Power Sources* **233**, 121–130 (2013).
54. de Biasi, L. *et al.* Between scylla and charybdis: Balancing among structural stability and energy density of layered NCM cathode materials for advanced lithium-ion batteries. *J. Phys. Chem. C* **121**, 26163–26171 (2017).
55. Kondrakov, A. O. *et al.* Anisotropic lattice strain and mechanical degradation of high- and low-nickel NCM cathode materials for Li-ion batteries. *J. Phys. Chem. C* **121**, 3286–3294 (2017).
56. Kondrakov, A. O. *et al.* Charge-transfer-induced lattice collapse in Ni-rich NCM cathode materials during delithiation. *J. Phys. Chem. C* **121**, 24381–24388 (2017).

57. Ryu, H.-H., Park, K.-J., Yoon, C. S. & Sun, Y.-K. Capacity fading of Ni-rich $\text{Li}[\text{Ni}_x\text{Co}_y\text{Mn}_{1-x-y}]\text{O}_2$ ($0.6 < x < 0.95$) cathodes for high-energy-density lithium-ion batteries: Bulk or surface degradation? *Chem. Mater.* **30**, 1155–1163 (2018).
58. Liu, H. *et al.* Spatially resolved surface valence gradient and structural transformation of lithium transition metal oxides in lithium-ion batteries. *Phys. Chem. Chem. Phys.* **18**, 29064–29075 (2016).
59. Yan, P., Zheng, J., Zhang, J.-G. & Wang, C. Atomic resolution structural and chemical imaging revealing the sequential migration of Ni, Co, and Mn upon the battery cycling of layered cathode. *Nano Lett.* **17**, 3946–3951 (2017).

Acknowledgements

This study is part of the projects being funded within the BASF International Network for Batteries and Electrochemistry. The work was partially carried out with the support of the Karlsruhe Nano Micro Facility (KNMF, www.knmf.kit.edu), a Helmholtz research infrastructure at Karlsruhe Institute of Technology (KIT, www.kit.edu). We thank Dr. Thomas Bergfeldt, Dr. Sabine Schlabach and Dr. Lea de Biasi, Dr. Reiner Mönig and Dr. Holger Gefßwein for ICP-OES, FIB-EDX and *operando* XRD measurements, respectively. This article has been funded through the Open Access Publishing Fund of Karlsruhe Institute of Technology.

Author Contributions

S.N. prepared composite electrodes, performed electrochemical experiments and evaluated data. A.M. prepared FIB cuts and performed TEM and EDX measurements. C.R. prepared the ALD coating. J.J. provided scientific guidance. S.N., A.M. and T.B. prepared the figures. S.N. and T.B. wrote the manuscript. S.N., P.H. and T.B. supervised the project. All authors reviewed the manuscript.

Additional Information

Supplementary information accompanies this paper at <https://doi.org/10.1038/s41598-019-41767-0>.

Competing Interests: The authors declare no competing interests.

Publisher's note: Springer Nature remains neutral with regard to jurisdictional claims in published maps and institutional affiliations.



Open Access This article is licensed under a Creative Commons Attribution 4.0 International License, which permits use, sharing, adaptation, distribution and reproduction in any medium or format, as long as you give appropriate credit to the original author(s) and the source, provide a link to the Creative Commons license, and indicate if changes were made. The images or other third party material in this article are included in the article's Creative Commons license, unless indicated otherwise in a credit line to the material. If material is not included in the article's Creative Commons license and your intended use is not permitted by statutory regulation or exceeds the permitted use, you will need to obtain permission directly from the copyright holder. To view a copy of this license, visit <http://creativecommons.org/licenses/by/4.0/>.

© The Author(s) 2019